

Near surface shear wave velocity profile development in the Pioneer Valley and Tufts campus using a coupled HVSR-MASW technique

Marshall Pontrelli

December 18, 2020

Abstract

Near surface geology plays an important role in earthquake ground motion estimation and thus is a vital area of study for infrastructure resilience. Soil profiles with lower velocity sediments overlying higher velocity bedrock will amplify energy at certain frequencies due to conservation of energy across an impedance boundary. This phenomenon is known as “site amplification” and the field of study related to near surface effects is the field of “site response”. To estimate site response, the NEHRP recommends a six-tiered system, denoted with letters A-F with F being the most and A being the least susceptible to site amplification. These tiers are based off a measure called “ V_{s30} ” which is the average shear wave velocity of the top 30 meters of soil. For example, low V_{s30} sites are classified as F or E and high V_{s30} sites are classified as A or B. Though this measurement is a good preliminary step, *it gives an incomplete description of seismic site effects*. Specifically, V_{s30} 1) does not provide the depth to the impedance boundary which will determine the frequency of shaking and 2) does not capture effects from soil deeper than 30 meters. In this study, I use two measurements, Multi-channel Analysis of Surface Waves (MASW) (Park 1998, 1999) and the Horizontal to Vertical Spectral Ratio (HVSR) (Nakamura, 1989) to provide greater constraint on site near surface S-wave velocity profile than V_{s30} alone. MASW estimates S-wave velocity profiles using surface wave dispersion and HVSR provides the site fundamental resonance, often in the engineering literature interpreted as multiple-reflecting S-waves and thus a proxy of the fundamental peak of the S-wave empirical transfer function. Traditionally, V_{s30} measurements are collected using MASW or similar methods but coupled with the HVSR, the MASW measurements are much more powerful. In the field, the addition of an HVSR measurement is easy and is well worth it for the S-wave profile improvement. I perform and analyze measurements at 3 sites, two in the Pioneer Valley near Springfield, MA in relatively deep river flood plain sediments and one on the Kraft Field at Tufts Campus in relatively shallow glacial outwash sediments.

1.0 Introduction

Upon arrival to the near surface, earthquake waves are amplified at certain frequencies depending on the soil-bedrock interface impedance contrast and the depth of the soil column (Thomson, 1950; Haskell, 1960; Borchardt, 1970; Kramer, 1996). In the field of site response, it is common to model this phenomenon as a simplified soil profile of laterally homogenous, horizontally layered media with frequency independent damping and subject to vertically propagating shear waves. These assumptions are collectively referred to as “SH1D” (the SH is the SH wave polarization and 1D is 1 dimensional propagation direction). Quantifying site response is essential to developing resilient infrastructure.

Normal incidence shear waves propagating vertically through an SH1D soil column amplify at each interface at

$$\left| \frac{u_i}{u_j} \right| = \frac{\rho_i \beta_i}{\rho_j \beta_j} \quad (1)$$

at frequencies

$$f_n = \frac{\beta_i}{4d_i} \quad (2)$$

where

u_i is the displacement of layer i

u_j is the displacement of layer j

ρ_i is the density of layer i

ρ_j is the density of layer j

β_i is the density of layer i

β_j is the density of layer j

d_i is the thickness of layer i

f_n is the fundamental frequency

From equation 1, which is referred to as the ‘‘impedance contrast’’ of the boundary between two layers, lower density and velocity soil overlying higher density and velocity basement rock will amplify the surface displacement relative to the basement displacement. Additionally, from equation 2, the fundamental resonance of shaking will decrease with an increase in depth or a decrease in overburden S-wave velocity.

The NEHRP site classification system is split up into 6 site classes, A-F each defined by a range of V_{s30} values (table 1). V_{s30} is defined as the average shear wave velocity of the top 30 meters of the soil profile and is computed using the equation:

$$V_{s30} = \frac{\sum_{i=1}^n d_i}{\sum_{i=1}^n \frac{d_i}{V_{s_i}}} \quad (3)$$

where n is the number of layers, d is the depth of layer i and V_s is the S-wave velocity of layer i . This computation is performed for only the top 30 meters of the soil profile to compute V_{s30} but can be used to compute the average S-wave velocity over any soil profile if the profile is not limited to only the top 30 meters.

Site Class	V_{s30} (m/s)	General Description
A	> 1500	Hard rock
B	760-1500	Rock with moderate weathering
C	360-760	Very dense soil and soft rock
D	180-360	Stiff soil
E	< 180	Soft clay soil
F	N.A	Soils requiring site specific evaluations

Table 1: NEHRP site classification system.

The NEHRP site classification system provides a good first approximation for site effects. It does not, however, capture some key information, specifically 1) depth to the significant impedance contrast and 2) S-wave velocity information below 30 meters. Consider the following two shear wave velocity profiles: profile 1 and profile 2 (figure 1).

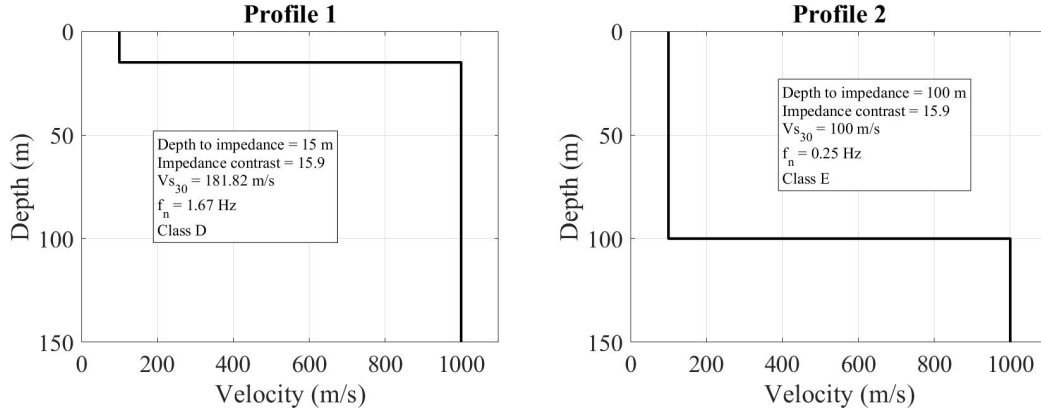


Figure 1: S-wave velocities for profiles 1 and 2. Shown are each profile's depth to the impedance contrast, impedance value (equation 1), V_{s30} (equation 3), f_n (equation 2) and site class (table 1).

Each has a single layer of 100 m/s S-wave velocity overlying a basement layer of 1000 m/s. Profile 1, however, is much shallower at a depth of 15 m whereas profile 2 is deeper at a depth of 100 meters. Because the basement velocity is incorporated into the V_{s30} computation for profile 1, the V_{s30} is greater than that of profile 2 and consequently, the site class is different: site class D instead of site class E. But is profile 1 less susceptible to site effects than profile 2 as its site classification would indicate? In fact, their impedances are the same and thus the maximum amplification of the site transfer function is the same, this maximum amplification simply occurs at a different frequency (figure 2, note the profile used to generate this figure includes soil damping of $\zeta = 2.5\%$ which lowers the impedance. With no soil damping, the transfer function amplification equals 15.9, the impedance in figure 1 computed from eq 1). Thus, the maximum amplification of each of these profiles will affect buildings of different heights, but in similar amounts of energy amplification. Using the back of the hand calculation of 0.1 s period per story to calculate building fundamental resonance, a 6-story building at profile 1 and a 40-story building at profile 2 will be most susceptible to amplification at its respective site. In each case, however, the amount of amplification at this frequency is the same and thus, I argue, the two profiles should have the same site classification.

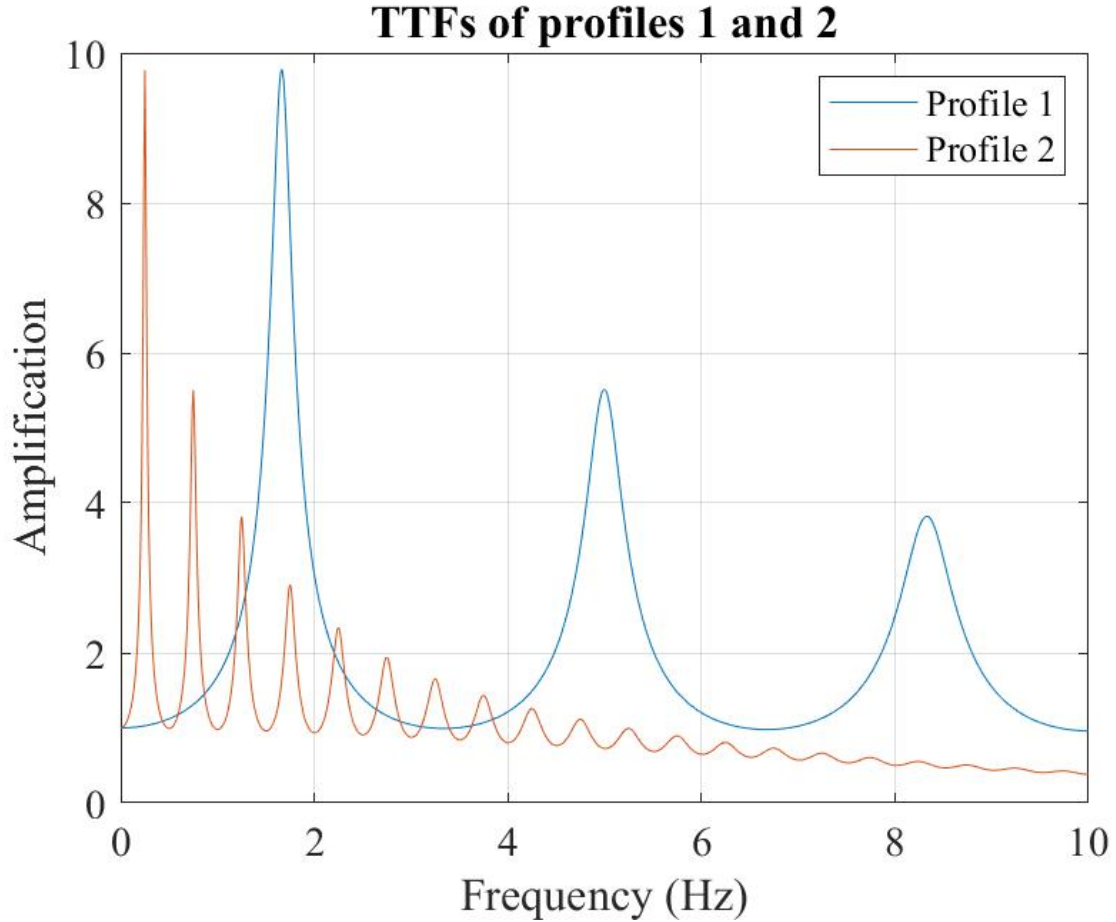


Figure 2: Theoretical transfer functions for profiles 1 and 2. The overburden and basement layer of each profile has a density of 1.7 and 2.7 g/cm³ respectively. The overburden damping value for each profile is $\zeta = 2.5\%$

2.0 Methods

In this study, I use two data collection and processing techniques, MASW and HVSR, and two forward models both based of Thompson Haskell Propagator matrices (Thompson 1050, Haskell 1953, Haskell 1960, Shearer 2017) to develop dispersion curves and SH1D theoretical transfer functions.

2.1 HVSR

2.1.1 Theory

The horizontal to vertical spectral ratio (HVSR) is an indirect way of approximating the surface-to-borehole empirical transfer function (ETF) from a single surface recording by canceling out the Rayleigh wave and P-wave influences on the surface record in order to enhance the image of the shear wave resonance (Nakamura, 1989). The surface ground motion is contaminated by surface waves, particularly Rayleigh waves, so the magnitude response at a site is not a clear representation of shear wave content in the record. The HVSR minimizes the effect of the Rayleigh wave on the surface recording to isolate the shear wave resonance,

thus approximating both the fundamental frequency and amplification of multiple reflecting SH waves. The amplification of vertically propagating shear waves is

$$a(f) = \frac{H_a}{H_b} \quad (4)$$

where H_a is the horizontal magnitude response at a site on the ground surface, and H_b is the horizontal magnitude response at a location at depth. This ratio is analogous to the surface-borehole transfer function. The surface site, H_a , is influenced by Rayleigh waves, the amount of which relative to the bedrock site is

$$\text{Influence of Rayleigh wave} = \frac{V_a}{V_b} \quad (5)$$

where V_a is the vertical magnitude response at the surface site, and V_b is the vertical magnitude response at the soil-bedrock interface site. This assumes that the Rayleigh wave particle ellipse dimensions are uniform and scaled throughout the material (Fig. 3, maroon lines). Dividing the shear wave amplification by the influence of the Rayleigh wave, therefore, removes the influence of the Rayleigh wave.

$$a(f)/\text{Influence of Rayleigh wave} = \frac{H_a}{H_b} * \frac{V_b}{V_a} \quad (6)$$

There is little amplification of multiple reflecting P-waves propagating from location the base to the surface at the shear wave resonant frequency (f_n) because the P-wave has a higher velocity than the S-wave, thus the P-wave f_n will be higher than the S-wave f_n . Similarly, Rayleigh waves influence the record at higher frequencies than the S-wave f_n . The ratio of the vertical motions at the S-wave f_n is therefore approximately 1, while at higher frequencies, the correction normalizes out the Rayleigh wave and P-wave influences. The Rayleigh and P-wave resonance peaks beyond the S-wave f_n are therefore diminished without significantly affecting the amplitude or shape of the fundamental peak. The S-wave f_n and amplification at the surface can therefore be approximated by the HVSR at the fundamental frequency (f_0) as

$$HVSR(f_0) = \frac{H_a}{V_a} \quad (7)$$

because $V_b/H_b = 1$. Equation 10 defines the horizontal to vertical spectral ratio.

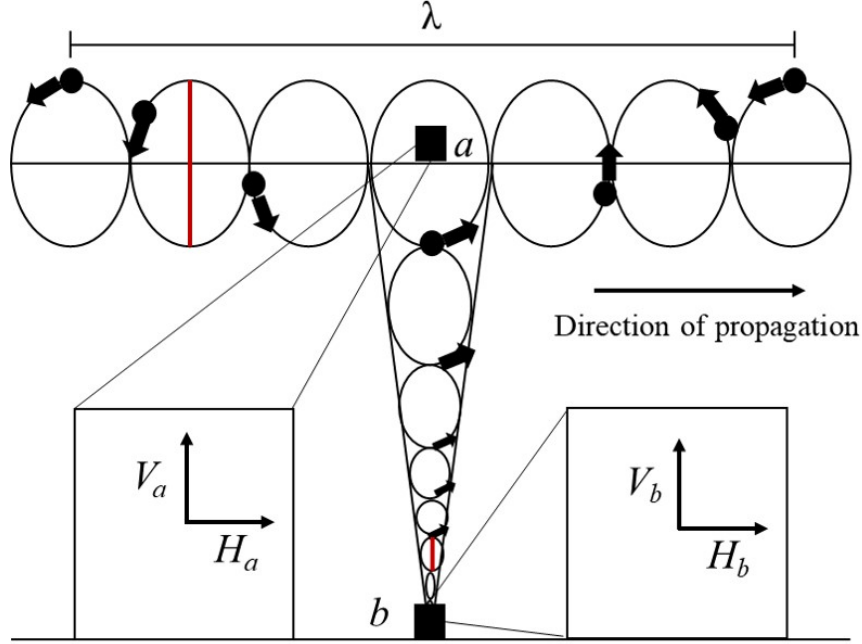


Figure 3: Retrograde Rayleigh waves traveling left to right across the page. The circles represent particles and the arrows represent their motion. The ellipses show the continuous particle motion. The squares represent locations a at the surface and b at depth. The maroon lines show the length of the long axis of the Rayleigh wave ellipse at location a and at location b . The Rayleigh wave cartoon is based on Fig. 2.15 in Sheriff and Geldart 1995, second edition.

2.1.2 Data Processing

I collect 30 minutes of data in the field and filter the raw record using a fourth-order bandpass Butterworth filter (Butterworth 1930) with a low corner of 0.1 Hz and a high corner of 49 Hz (figure 4). I then window the data into 120 second windows, 1 second apart and compute the Fourier amplitude spectra of each component of each window. I then combine the horizontal components using their geometric mean (SESAME 2004a) and smooth the resulting horizontal and magnitude response vertical magnitude response using a 0.5 Hz width smoothing filter (figure 5a and b). I then divide the components to get an HVSR of each window (figure 5c) and stack the 14 HVSRs and average them together using the log-normal maximum likelihood estimator (figure 5d): (Thompson et al. 2009, Thompson et al. 2012, Steidl et al. 1996).

$$HVSR_{avg} = \exp\left(\frac{1}{n} \sum_{i=1}^n \ln[HVSR_i(f)]\right) \quad (8)$$

where $HVSR_i(f)$ is the HVSR(f) for $i = 1, \dots, n$ windows. I plot $HVSR_{avg}$ with a large sample $100(1 - \alpha)$ confidence interval:

$$\exp(\ln[HVSR_{avg}(f)] \pm z_{1-\alpha/2} * \sigma_{\ln}(f)) \quad (9)$$

with standard deviation:

$$\sigma_{\ln}(f) = \sqrt{\frac{1}{n} \sum_{i=1}^n (\ln[HVSR_i(f)] - \ln[HVSR(f)])^2} \quad (10)$$

Finally, I measure different shapes in the HVSr fundamental peak (figure 5e).

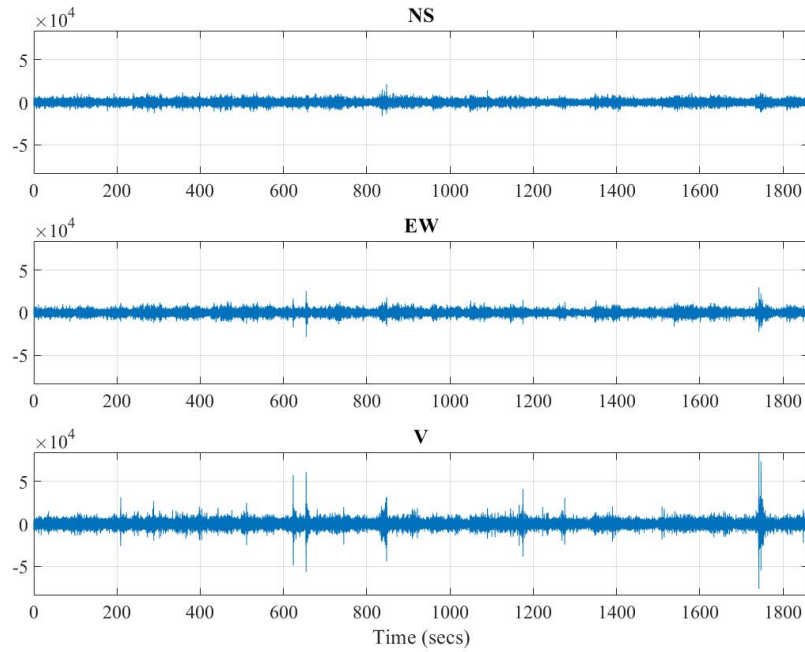


Figure 4: Microtremor time series after processing.

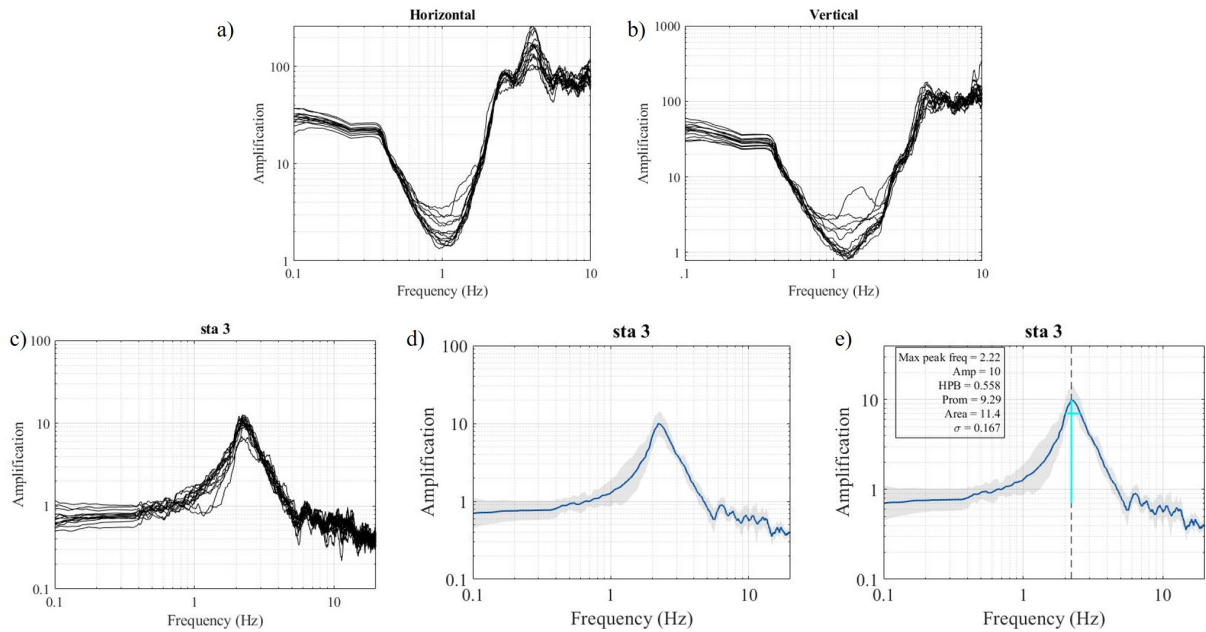


Figure 5: Entire process of developing an HVSr. a and b) computing horizontal and vertical Fourier amplitude spectra of each window. c) computing the HVSr at each window. d) averaging the HVSr and computing its confidence intervals using eqs 8-10. e) computing statistics describing the shape of the peak.

2.2 MASW

2.2.1 Theory

MASW, or multichannel analysis of surface waves, is a processing technique to pull wave dispersion information out of a geophone line. The theory is laid out in Park et al. 1998b and begins in the (x-t) domain with a geophone line shot gather. Each channel is transformed into the frequency domain using the Fourier transform:

$$U(x, w) = \int u(x, t)e^{iwt} dt \quad (11)$$

It is then split into the phase and magnitude response:

$$U(x, w) = P(x, w)A(x, w) \quad (12)$$

where $P(x, w)$ is the phase and $A(x, w)$ is the amplitude spectrum. $P(x, w)$ contains all the phase information so we break down eq. 11 further into:

$$U(x, w) = e^{-i\phi x} A(x, w) \quad (13)$$

where $\Phi = w/c_w$, w = circular frequency in radians and c_w = phase velocity at frequency w . We then apply the transform:

$$V(w, \phi) = \int e^{-i(\Phi-\phi)x} [A(x, w)/|A(x, w)|] dx \quad (14)$$

Thus, by looping over values of ϕ at each frequency, the maximum value of $V(w, \phi)$ will be w/c_w from which we can solve for the phase velocity c_w at the correct frequency (these equations are provided in more detail in Park 1998b).

2.2.2 Data Processing

To compute dispersion curves practically in the field, I collect a shot gather with 2 meter offset and 1 meter spacing using a geophone line of 24 4.5 Hz geophones collected using a Seistronix data acquisition unit and a sledgehammer trigger. I then process the data using eqs. 11-14. A time domain plot of a gather is shown in figure 6a below and the corresponding dispersion curve is figure 6b. I then select the maximum value of the fundamental mode in the dispersion curve to develop my final dispersion curve (figure 6c).

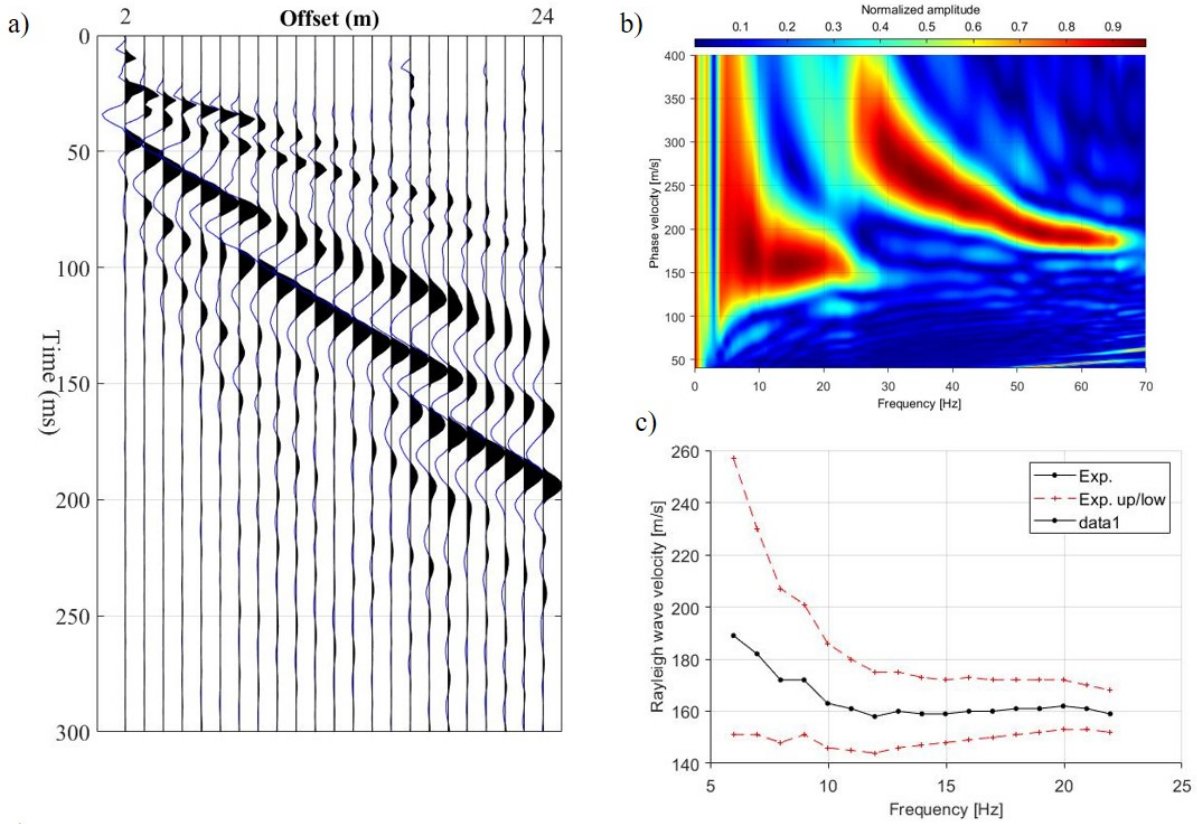


Figure 6: a) Shot gather for MASW processing. b) dispersion curve from shot gather in a. c) dispersion curve picks from b.

2.3 SH1D TTF using Boore (2005) software

2.3.1 Theory

In site response studies, we often model the theoretical transfer function, hereafter TTF, with 1) vertically propagating shear waves through 2) laterally homogenous soil layers that have 3) frequency independent damping and 4) strain independent shear modulus, assumptions collectively referred to as “SH1D”. The source input $i(t)$, earth’s crust $h_e(t)$, site geology $h_g(t)$, and instrument response $h_r(t)$ are linear time invariant systems, and the recorded ground motion $s(t)$ is a linear combination of these systems (figure 7):

$$s(t) = i(t) * h_e(t) * h_g(t) * h_r(t) \quad (15)$$

where $*$ is the convolution operator (Borchert, 1970; Sheriff and Geldart, 1995). The Fourier response spectra of the ground motion is equal to the product of the Fourier transform of each of the respective systems:

$$S(f) = I(f)H_e(f)H_g(f)H_r(f) \quad (16)$$

An earthquake at a large hypocentral distance from the location of interest has vertically incident incoming waves due to Snell’s law and the tendency of density to increase with depth in the Earth (Sheriff and Geldart, 1995). Two records in the basin, a on soil and b , on rock have equal source, path and instrument response, thus the shear wave transfer function, $a(f)$, from location b to location a is the ratio of the magnitude response spectra of the horizontal component of a and b .

$$a(f) = \frac{S_{ha}(f)}{S_{hb}(f)} \quad (17)$$

where $S_{ha}(f)$ is the horizontal component of the record at location a and $S_{hb}(f)$ is the horizontal component of the record at location b . This ratio is the site SH1D transfer function and we can model it using a forward model or approximate it using data.

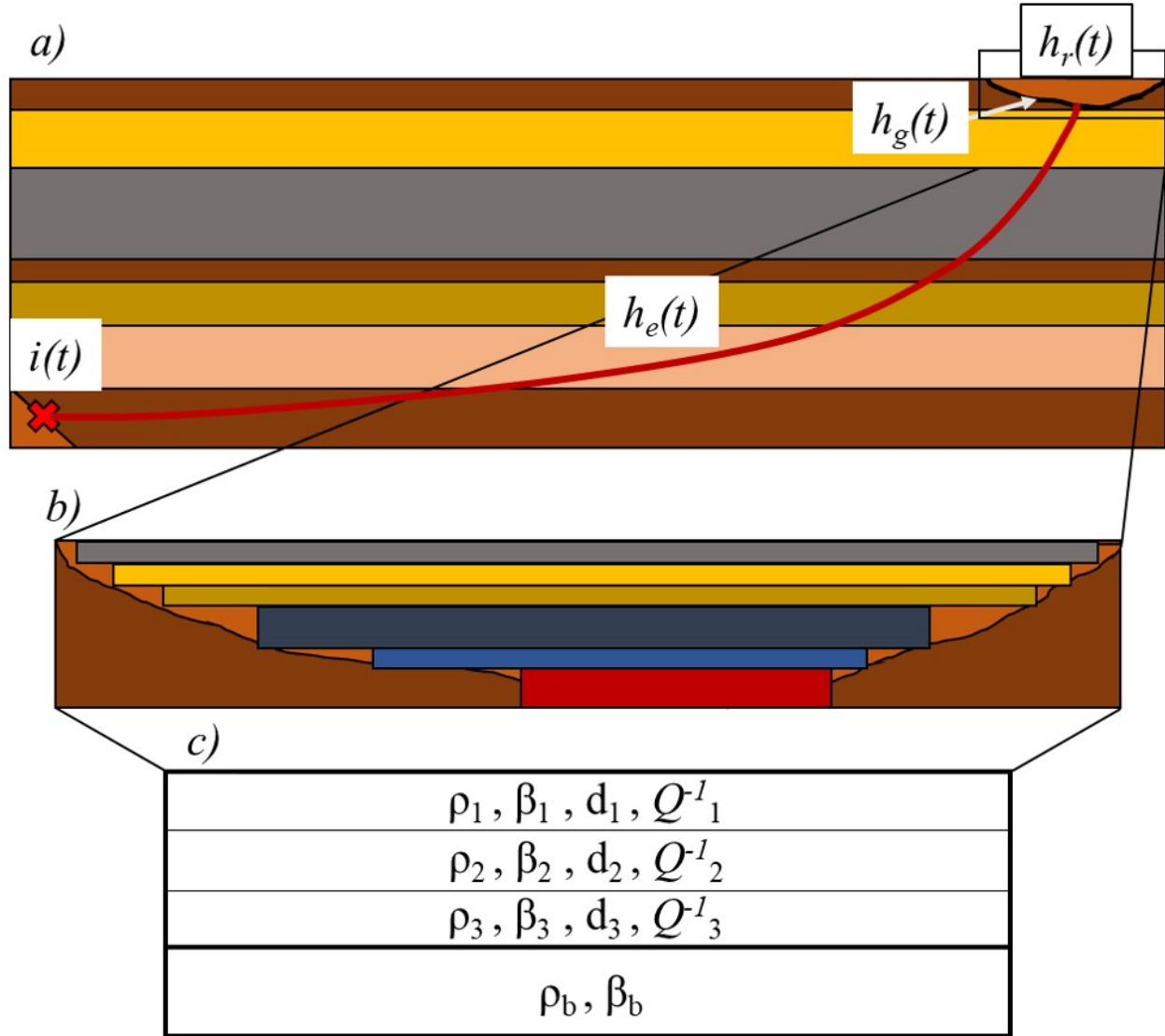


Figure 7: a) Site response model from a global seismological perspective with earthquake hypocenter, $i(t)$, represented by a red x, earth's crust, $h_e(t)$, represented by horizontal layers of varying color, site geology, $h_g(t)$, represented by a brown basin, and instrument response, $h_r(t)$, represented by a black square. b) The site geology, $h_g(t)$. c) The variables with which we model the site geology.

The SH1D TTF is a function of the vibrational properties of the media through which the waves propagate: the depth d , the shear wave velocity β , the density ρ and the attenuation Q of the overburden, and the velocity and density of the basement. For a more in depth discussion of Q see Shearer 2019.

2.3.2 Computation

To compute the theoretical transfer function, I use the Nratle Fortran routine, which calculates the Thomson-Haskell plane SH-wave transfer function (Thomson, 1950; Haskell, 1953) for horizontally stratified, laterally homogenous layers with vertically propagating shear waves (written by C. Mueller with modification by R. Herrmann and distributed in the Boore (2005) SMSIM ground motion simulation program). The input parameters for Nratle are a shear wave velocity profile (β), and corresponding depths (d), densities (ρ) and attenuations (iQ_s) of the overburden; and the density and shear wave velocity of the basement. The outputs of Nratle are the TTF amplification as a function of frequency in Hz and is used to compute the curves in figure 2.

3.0 Data

In this project, I use data from three sites, two in the Connecticut River Valley and one on the Tufts campus. At each of these sites, I collected and processed microtremor data for the HVSR and geophone traces to compute dispersion curves.

3.1 L62A

L62A was a transportable array station installed as part of the Earthscope project from 2013-2015. It is located on Connecticut river flood plain sediments about 10 km south of Springfield. I found the local site conditions to be swampy and the property it is on is farmland. A former undergraduate student at Tufts, Justin Reyes, originally identified the site as exhibiting site amplification during a search for resonant New England seismological stations he performed in 2019. This site is the only site of the three where instead of collecting microtremor data, I used the data from the TA station.

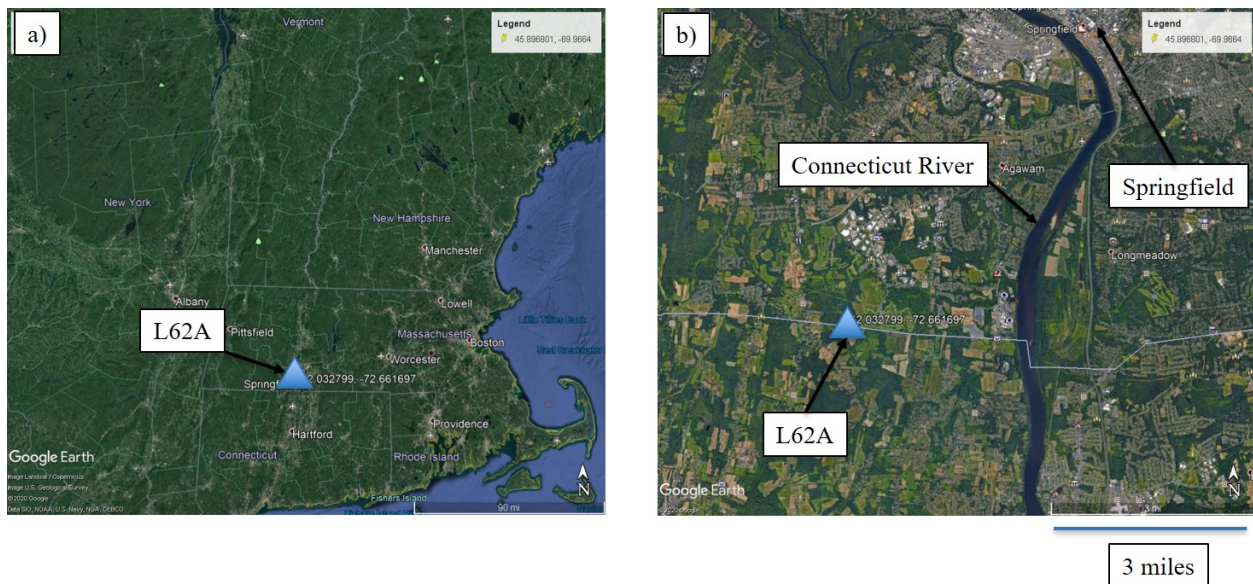


Figure 8: a) Location of L62A within the Connecticut River Valley b) Higher resolution image showing surrounding farmland on Connecticut River flood plain



Figure 9: a) The field where L62A is, to the right and running behind the car is swampy, wet lowland. a) L62A site.

3.2 Memorial Bridge

The Memorial Bridge site is located just south of Memorial Bridge in Springfield on the East side of the Connecticut River between the River and Route 91. Like L62A, it sits on the Connecticut River flood plain sediments. It is adjacent to a train line and surrounded by various types of infrastructure: highway, bridge, parking lot and others.

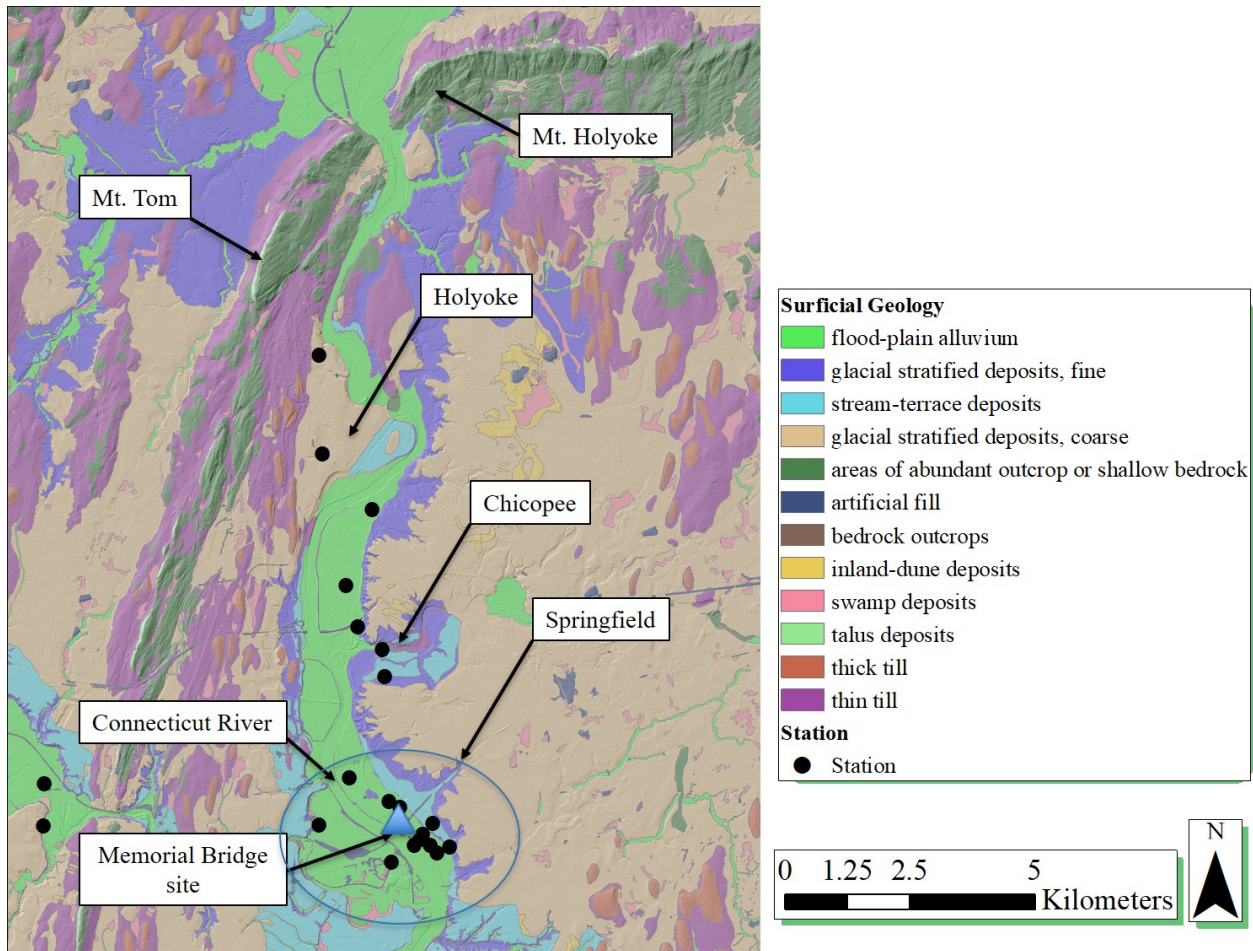


Figure 10: Memorial Bridge location within the greater area surficial geology



Figure 11: a) Memorial bridge site adjacent train line b) Site with Memorial Bridge in the distance and downtown Springfield to the right

3.3 Kraft Field

The Kraft field site is on the Tufts Medford-Somerville campus. The main portion of the campus (thick till in figure) is a drumlin and the surrounding lower regions are a combination on artificial fill and glacial outwash deposits. This site is located is located on about 6 meters of outwash deposits (figure 13) known from drilling studies in Grant Garven's hydrogeology class.

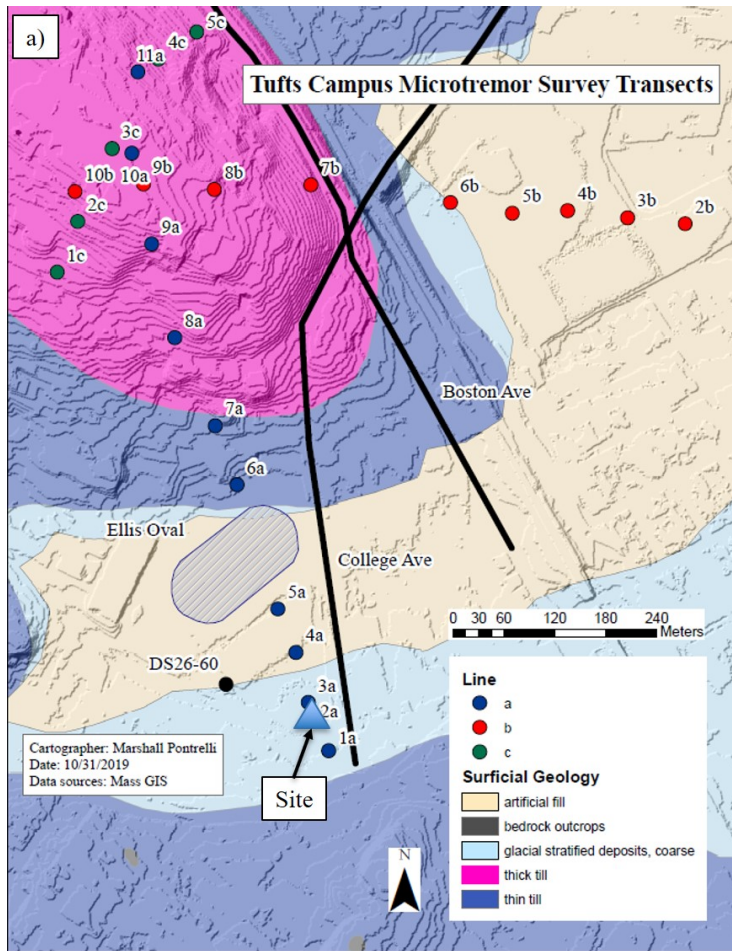


Figure 12: a) Kraft field site within local surficial geology b) Site

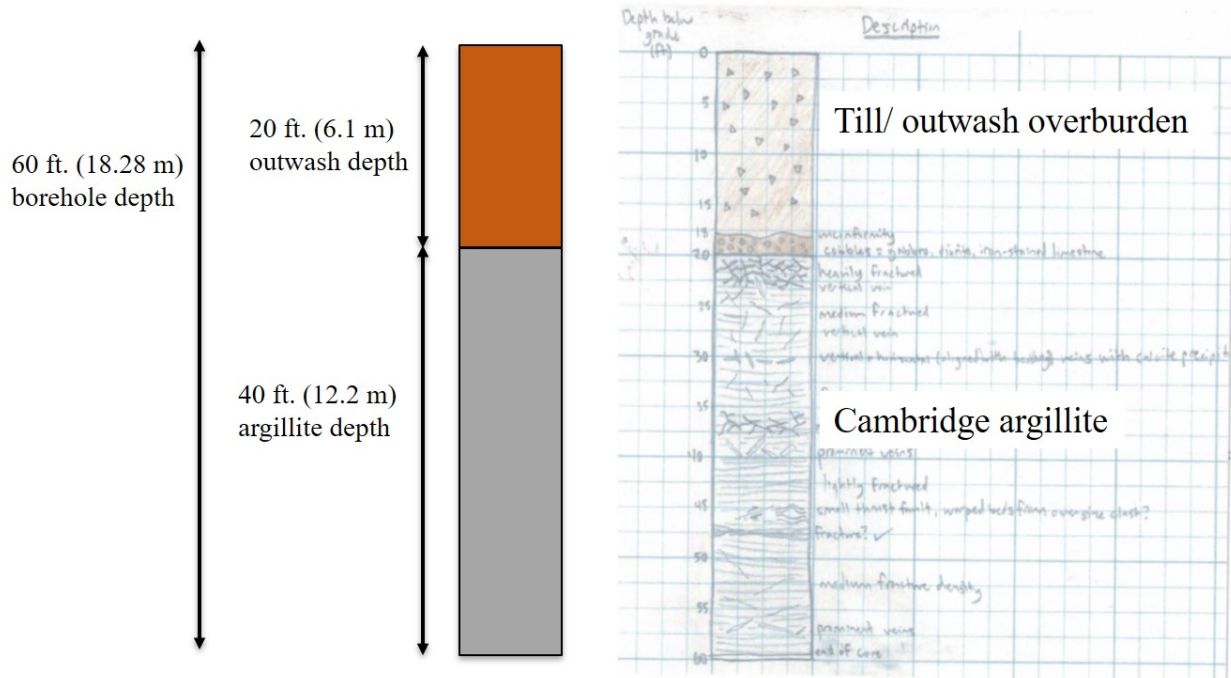


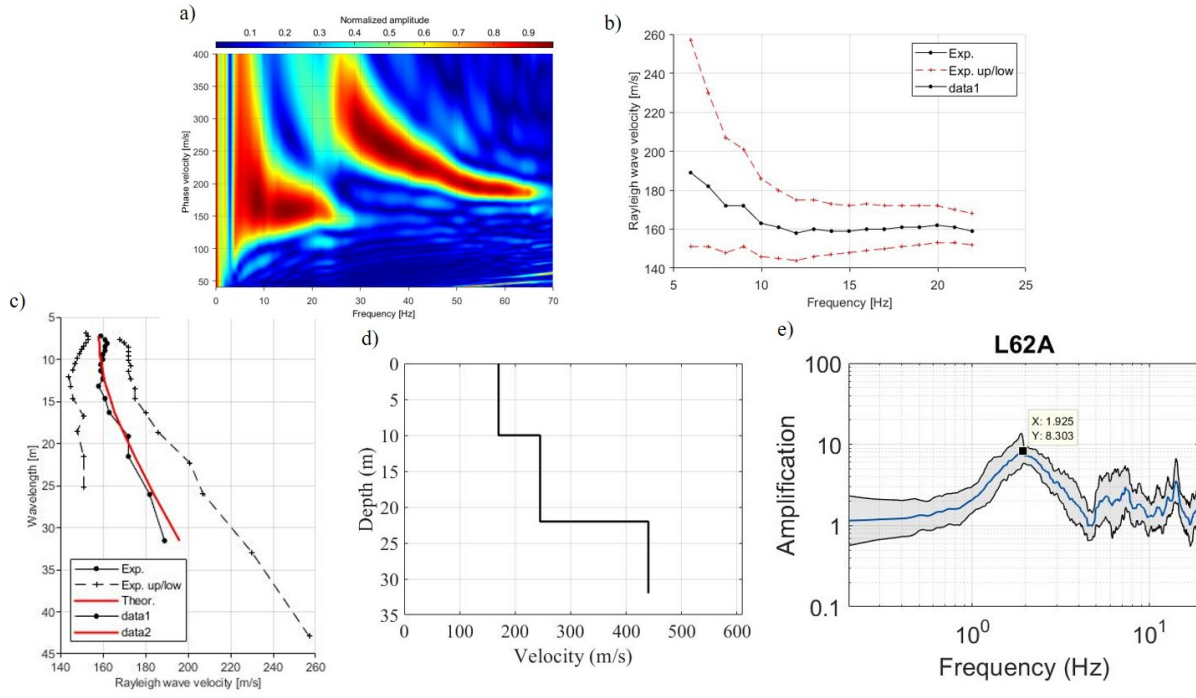
Figure 13: Kraft Field well log from nearby site DS26-60 (figure) drawn by Grant Garven and reinterpreted by me.

4.0 Results

For each of the three sites, I developed an HVSR and a dispersion curve and inverted for the shear wave velocity profile that fits the relationship in equation 2. This yields a 1) a depth to the impedance contrast, 2) a fundamental frequency (computed from the data) and 3) and average velocity to the impedance contrast. I also present the V_{s30} when the depth is greater the 30 meters (which is only at one site).

4.1 L62A

The dispersion curve for station L62A is clean with a clear fundamental and first mode. The higher modes were clear too but are not shown in the figure. The fundamental phase velocities are just below 200 m/s. The model I got that best fit this dispersion curve while conforming to the site fundamental resonance is a roughly linearly increase shear wave velocity profile of 32 meters depth with an average velocity of 245.15 m/s. This has a V_{s30} of 238.12 m/s and is, by the traditional classification scheme, a site class D.

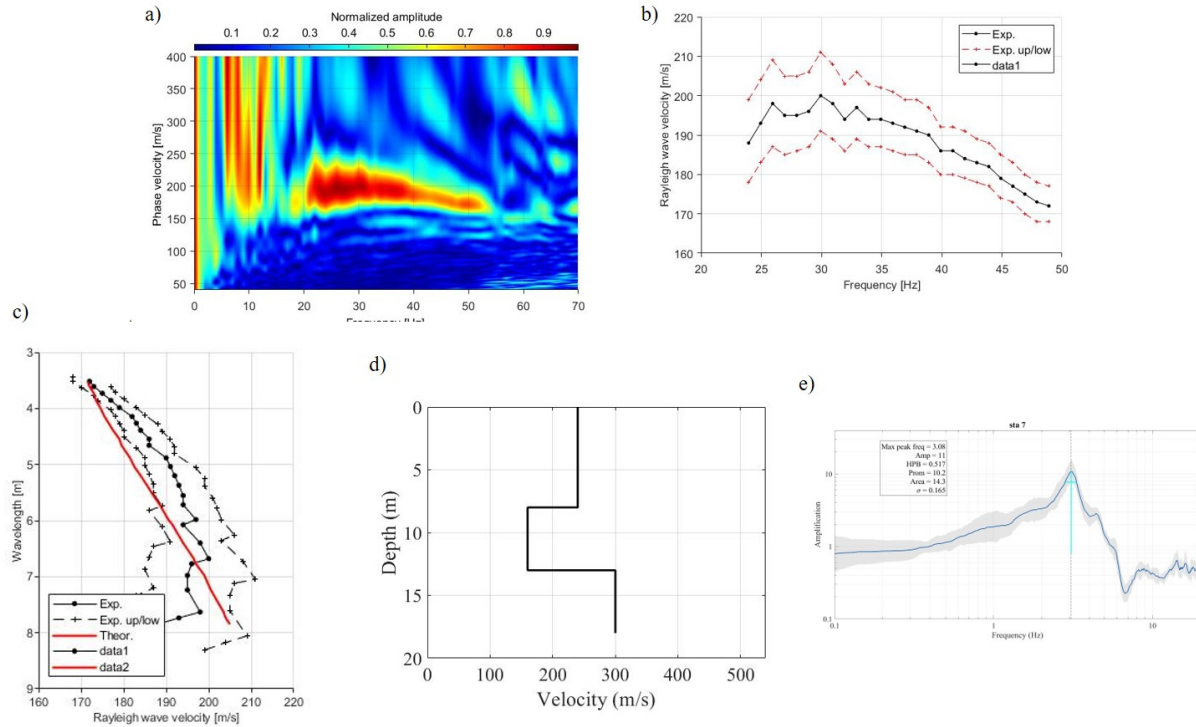


Station	Depth (m)	f_n	Vs_{avg} (to impedance interface m/s)	Vs_{30} m/s	Site class
L62A	32	1.925	245.1536	238.1237	D

Figure 14: a) Dispersion curve b) dispersion curve picks c) model fit d) shear wave velocity profile from the model e) HVSR curve. Table) Results from analysis

4.2 Memorial Bridge

The Memorial bridge dispersion curve is significantly less clean than the L62A dispersion curve. There is no clear evidence of higher modes and at frequencies below 20 Hz, the signal becomes incoherent. There is, however, a clear fundamental mode at around 200 m/s. This mode, however, is concave down, indicating a potential low velocity zone. Consequently, the model fit for this profile is not as good as the model fit for L62A as I was unable to map the low velocity zone cleanly onto the dispersion curve. Despite the inability to get a tight fit, however, we still get a good picture of the average shear wave velocity of the site of 221 m/s, like that obtained at L62A. These sites are located in the same soil unit and thus it makes sense that their average velocities are similar even though the Memorial bridge site is messier. My guess is that the mess at Memorial Bridge is from the many infrastructural projects that have shaped and reshaped the subsurface.



Station	Depth (m)	f_n	Vs_{avg} (to impedance interface m/s)	Vs_{30} m/s	Site class
Memorial Bridge	18	3.07	221.5385	N/A	D

Figure 15: a) Dispersion curve b) dispersion curve picks c) model fit d) shear wave velocity profile from the model e) HVSR curve. Table) Results from analysis

4.3 Kraft Field

The Kraft Field site is in a different geologic unit than L62A and Memorial bridge, glacial outwash instead of river flood plain. There is evidence of the first mode in the dispersion curve, though is less clean than the first mode in the L62A dispersion curve. Additionally, the phase velocities are significantly higher, between 300 and 800 m/s than the phase velocities in the other two sites with more steeply increasing phase velocities towards lower frequencies. This, combined with a much higher fundamental frequency of 12 Hz yields a shallower, higher shear wave velocity profile than the other two sites. The 6.5 meters I calculated for the depth from the dispersion curve inversion is close to the 6 meters at the DS26-60 site that was found from drilling a borehole, a good indicator that the inversion is pretty close to the actual profile.

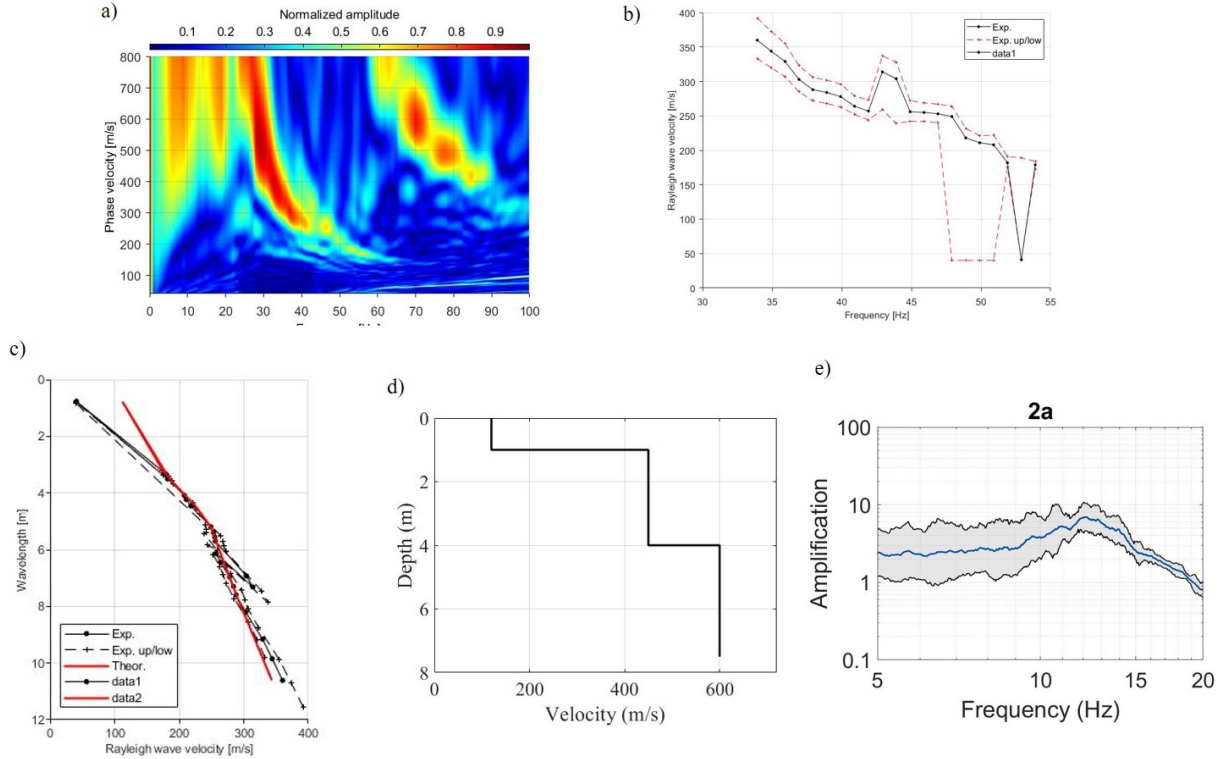


Figure 16: a) Dispersion curve b) dispersion curve picks c) model fit d) shear wave velocity profile from the model e) HVSR curve. Table) Results from analysis

5.0 Discussion and conclusion

Using this combination of MASW dispersion inversion and HVSR fundamental frequency, I can compute easily the depth and average shear wave velocity of a site, giving a better picture of the subsurface than $V_{S_{30}}$ in isolation. At the 3 sites studied in this project, the technique showed that at sites L62A and Memorial Bridge, both within the Connecticut River flood plain sediments, the shear wave velocity profiles and depths are similar, though the finer details of each site's profile can be more complex. The inversion scheme works for the Kraft field as well, obtaining higher velocities in the profile while predicting a depth close to a known depth nearby. At each of the sites, I measured the fundamental site resonance using the HVSR and inverted for the site shear wave velocity ensuring the relationship in eq. 2 was maintained. This yields, in addition to fundamental resonance, average shear wave velocity and depth to the impedance contrast. These three parameters, I think, better describe a site than $V_{S_{30}}$ in isolation because they account for frequency of shaking and depths greater than 30 meters in a profile, providing engineers with a more complete picture of the profile. Additionally, this technique only requires slightly more time, effort and equipment than a $V_{S_{30}}$ measurement alone with the addition of 30 minutes of microtremor collection and HVSR processing, a well-studied and easy process. The additional information this classification system provides allows for better understanding of site resonance at a minimal extra cost than $V_{S_{30}}$ in isolation.

References

- Boore, D. M. (2005). SMSIM-Fortran Programs for Simulating Ground Motion from Earthquakes: Version 2.3-A of OFR 96-80-A. United States Department of the Interior. U. S Geological Survey.
- Borcherdt, R.D., (1970). Effects of Local Geology on Ground Motion Near San Francisco Bay. Bulletin of the Seismological Society of America. Vol. 60, No. 1, pp. 29-61.
- Butterworth, S., (1930). On the theory of filter amplifiers. Exp. Wirel. Wirel. Eng. 7, 536–541.
- Haskell N. A. (1953) The dispersion of surface waves on multilayered media. Bulletin of the Seismological Society of America; 72:17–34.
- Haskell, N. A. (1960). Crustal Reflection of Plane SH Waves. Geophysical Research 65(12): 4147-4150.
- Kramer, S.L. (1996). Geotechnical Earthquake Engineering, Prentice Hall, Upper Saddle River, N.J.
- Nakamura, Y. (1989) A Method for Dynamic Characteristics Estimation of Subsurface using Microtremor on the Ground Surface. Railway Technical Research Institute 30(1): 25-33.
- Olafsdottir, E.A., Erlingsson, S., Bessason, B. (2017). Tool for analysis of multichannel analysis of surface waves (MASW) field data and evaluation of shear wave velocity profiles of soils. Can. Geotech J. 55: 217-233 (2018).
- Park, C.B., Miller, R.D., Xia, J. (1998b). Imaging dispersion curves of surface waves on multi-channel record. Kansas Geological Survey.
- Park, C.B., Miller, R.D., Xia, J. (1999). Multichannel analysis of surface waves. Geophysics Vol 64, No.3, p. 800-808.
- SESAME (2004a). Guidelines for the implementation of the H/V spectral ratio technique on ambient vibrations. European Commission - Research General Directorate.
- SESAME (2004b). Site Effects Assessment Using Ambient Excitations. European Commission - Research General Directorate. Project No. EVG1-CT-2000-00026 SESAME.
- Shearer, P.M. (2019) Introduction to Seismology, 3rd edition. Cambridge University Press.
- Sheriff, R.E., Geldart, L.P. (1995). Exploration Seismology, Second Edition. Cambridge University Press.
- Steidl JH, Tumarkin AG, Archuleta R.J. (1996) What is a reference site? Bulletin of the Seismological Society of America 1996;86(6):1733–48.
- Thomson WT. (1950). Transmission of elastic waves through a stratified solid. Journal of Applied Physics: 21:89–93.